

Rod motifs in neutron scattering in spin ice

Claudio Castelnovo¹ and Roderich Moessner²

¹*TCM Group, Cavendish Laboratory, University of Cambridge,
J. J. Thomson Avenue, Cambridge CB3 0HE, United Kingdom*

²*Max-Planck-Institut für Physik komplexer Systeme, Nöthnitzer Str. 38, 01187 Dresden, Germany*

In classical and quantum spin ice, rod-like features appear in the neutron scattering structure factor when the pinchpoints characteristic of classical spin ice get washed out. We show that these features do *not* indicate the absence of spin correlations between planes perpendicular to the rods. Rather, they arise because neutron scattering is largely insensitive to the three-dimensional correlations which are present throughout. We present two very simple models which exhibit a pristine incarnation of such scattering rods. This provides a physical picture for their appearance, elucidates the role played by monopole excitations and identifies conditions conducive to their observation.

Spin ice¹ is arguably the only three dimensional magnetic material for which fractionalisation and the presence of an emergent gauge field have been established². Neutron scattering studies have played a central role, not least in pinning down qualitatively important features such as the pinch points³⁻⁵ and Dirac strings^{6,7}, indicating the presence of an emergent gauge structure.

Recently, many studies of potential quantum spin ice compounds have extended these investigations. One resulting observation is that in these systems, the pinchpoints are less well-defined. This is an important observation, as it is believed to be related to the presence of fractionalised monopole excitations: these are sources and sinks of the emergent gauge field, and as such degrade the conservation law responsible for the appearance of the pinch points.

As pinch points get washed out, they leave behind somewhat uniform, one-dimensional motifs, as observed in the classical spin ice compound Dy₂Ti₂O₇⁴, as well as the candidate quantum spin ices Pr₂Zr₂O₇⁸ and Nd₂Zr₂O₇^{9,10}, with concomitant observations in quantum Monte Carlo simulations¹¹; representative plots are reproduced in Fig. 1 from Refs 8, 9, and 11. Such scattering rods are not unheard of in pyrochlore compounds – indeed, for Gd₂Ti₂O₇ rods have also been sighted and successfully related to the presence of uncorrelated planes, whose normal is given by the rod direction¹².

This raises the twin questions of (i) how to account for the role of monopoles in the genesis of the scattering rods and (ii) how their presence leads to decorrelation between planes in the spin ice context.

The answer to the second question is that the rods do not in fact indicate decorrelated planes. Rather, three-dimensional correlations persist which are hidden by the matrix elements characteristic of the neutron scattering process. We demonstrate this by presenting two very simple models, neither of which exhibits decoupled planes but which do show rods in neutron scattering: the first is studied in Monte Carlo simulations while the second is a fully tractable analytical calculation for a single tetrahedron. The numerical model has the absence of doubly-charged monopoles as its sole ingredient, while tetrahedra without, or with a singly-charged, monopole are treated

as degenerate. The single-tetrahedron analytics straightforwardly relates the rods to properties of the classical interaction matrix for spin ice.

This demonstrates that the rod-like features persist in a regime far removed from the dilute monopole limit, where an emergent gauge field is a natural degree of freedom; their role is above all to decorrelate spins in neighbouring tetrahedra from one another, so that the single tetrahedron result agrees with that of the full lattice with doubly-charged monopoles suppressed.

We discuss the settings in which this condition is approximately met. These include quantum spin ice materials at intermediate energies, as well as classical spin ice at intermediate temperatures.

Models and results. We first show results from Monte Carlo simulations of classical dipolar and nearest-neighbour spin ice,

$$H = -J \sum_{\langle i,j \rangle} \vec{S}_i \cdot \vec{S}_j + D \sum_{i,j} \left[\frac{\vec{S}_i \cdot \vec{S}_j}{|\vec{r}_{ij}|^3} - \frac{3(\vec{S}_i \cdot \vec{r}_{ij})(\vec{S}_j \cdot \vec{r}_{ij})}{|\vec{r}_{ij}|^5} \right] \quad (1)$$

as well as single tetrahedron calculations. For the nearest-neighbour case we choose $J = 9$ K and $D = 0$, whereas for the dipolar case we use $J = -3.72$ K and $D = 1.41$ K; the distances \vec{r}_{ij} are measured in units of the pyrochlore nearest-neighbour distance.

We compare: (i) Monte Carlo simulations for the nearest-neighbour and dipolar spin ice models at high temperature; (ii) simulations of non-interacting spins subject to the hard constraint that all-in and all-out tetrahedra are strictly forbidden (no double monopoles); and (iii) a single tetrahedron calculation that accounts only for 2in-2out and single monopole configurations (i.e., double monopoles are forbidden). The results, in the form of neutron scattering structure factor,

$$\mathcal{F} = \sum_{\alpha, \beta = x, y, z} \left(\delta_{\alpha\beta} - \frac{k_\alpha k_\beta}{k^2} \right) \sum_{i,j} e^{i\vec{k} \cdot \vec{r}_{ij}} \langle S_i^\alpha S_j^\beta \rangle, \quad (2)$$

are shown in Fig. 2.

Our central observation is that these plots of the structure factor – from the high-temperature Monte Carlo simulations, the ideal lattice model without doubly-

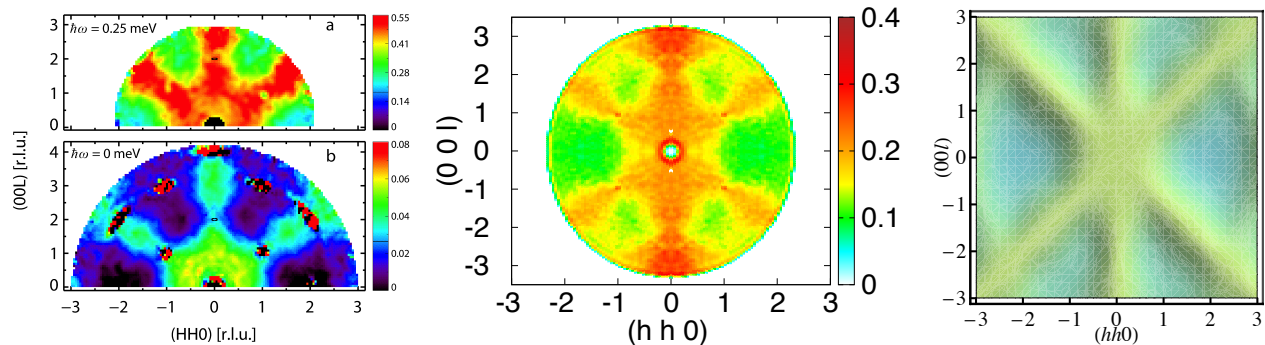


FIG. 1. Rod features in neutron scattering in the [200] and [111] directions in reciprocal space [where (r.l.u.) represents reciprocal lattice units]. Left panel: inelastic and elastic neutron scattering (top/bottom portion of the panel) on $\text{Pr}_2\text{Zr}_2\text{O}_7$ from Ref. 8. Middle panel: inelastic neutron scattering on $\text{Nd}_2\text{Zr}_2\text{O}_7$ from Ref. 9. Right panel: neutron scattering structure factor obtained from quantum Monte Carlo simulations of quantum spin ice (XXZ Hamiltonian) from Ref. 11.

charged monopoles, and the single-tetrahedron calculation – resemble each other strongly. We can thus use the analytical result from the latter to describe the rods, and the physical picture provided by the lattice model to identify the single most important ingredient for the genesis of the rods: the singly-charged monopoles do indeed remove the pinch points; but the suppression of the doubly-charged ones leaves the rods behind.

Let us now analyse the form of the correlations in more detail. The calculation (iii), presented in App. A, yields

$$\mathcal{F}_{\text{s.t.}}(\vec{k}) \propto \frac{1}{k^2} \left[k_x^2 c_y c_z + k_y^2 c_z c_x + k_z^2 c_x c_y + k_x k_y s_x s_y + k_y k_z s_y s_z + k_z k_x s_z s_x \right], \quad (3)$$

where $c_\alpha = \cos(\pi k_\alpha/2)$, $s_\alpha = \sin(\pi k_\alpha/2)$, and the vectors \vec{k} are expressed as customary in reciprocal lattice units (r.l.u.).

In particular in the [001] direction, $\vec{k} = (0, 0, k_z)$, Eq. (3) simplifies to a constant, which in real space is of course just a delta function describing uncorrelated planes. This, however, is not the full story. Replacing the neutron scattering transverse projector, linking spin correlations to the neutron scattering cross section, with a delta function yields the $\langle \vec{S}(\vec{q}) \cdot \vec{S}(-\vec{q}) \rangle$ structure factor in the left panel of Fig. 3. The rods have disappeared, and the correlations in the [001] direction look no weaker than those in other directions. It just so happens, for the directions of the rods, that the correlations are purely longitudinal, and therefore invisible to the neutrons on account of the transverse projector which comes along with the scattering matrix elements. While the three-dimensional nature of the correlations in the presence of scattering rods is therefore – of course – not at variance with any principle of physics, we believe that this is a rare instance in which a scattering rod does not go along with the emergence of $d - 1$ dimensional correlations. In a larger view of reciprocal space, this is directly evident: the rods do not get replicated in higher Brillouin zones.

Next, we turn to the broader implications of the relative success of the simple model calculation based on a

single tetrahedron. A priori, one would expect a single tetrahedron calculation to have a chance of being accurate if correlations beyond n.n. distance are small. This is obviously the case at high temperatures, where the leading term in a series expansion is just

$$\langle S_i^\alpha S_j^\beta \rangle \propto -H_{ij}^{\alpha\beta} / T. \quad (4)$$

Hence, to the degree that the correlations remain short-ranged, one might hope that a single-tetrahedron based calculation also remains accurate.

There is a further simplification for spin ice. For a single tetrahedron, the average over single-monopole states encodes no pair correlations, as half the bonds are frustrated and half satisfied in each state. In addition, the average over all $2^4 = 16$ configurations, corresponding to infinite temperature, also vanishes. This implies that the all-in and all-out correlations are just the negative of those over the six ice-rule obeying configurations. The former in turn is closely related to simply the adjacency (i.e., the Hamiltonian) matrix of the interaction cluster.

In other words, the presence of the monopoles effectively cuts off the correlations at nearest-neighbour distance; from where the only form of the correlations allowed by symmetry are those given by the adjacency matrix – thence the relation between correlations and the Hamiltonian matrix in Eq. (4).

Conclusions and outlook. Our simple insight is that rod-like motifs become more pronounced as single monopole excitations are mixed into the 2in-2out states, while double monopoles remain sparse. We expect the following ingredients to be conducive to generating such a situation. (i) At a purely classical level, the energy cost of double monopoles is four times larger than single monopoles, and their relative Boltzmann suppression produces an intermediate temperature regime where single monopoles are relatively dense while double ones are negligible; this corresponds to the broadening of pinch points at finite temperature in classical spin ice compounds⁴. (ii) The spin flip matrix elements in inelastic neutron scattering favour at low temperatures fluctuations between 2in-2out states and 3in-1out and 3out-1in

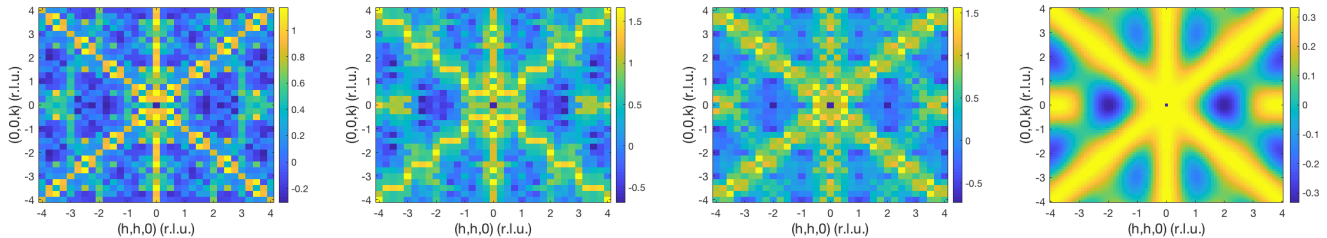


FIG. 2. Rods in neutron scattering resulting from four different models: First/second panel: Monte Carlo simulations for $L = 8$ on dipolar ($J = -3.72$ K, $D = 1.41$ K, $T = 10$ K) and nearest-neighbour ($J = 9$ K, $T = 10$ K) spin ice; Third panel: Stochastic sampling over spin ice configurations where double monopole tetrahedra are strictly forbidden, also for $L = 8$. Right Panel: Single tetrahedron calculation, summed uniformly over all configurations but the all-in and all-out ones.

states, whereas the appearance of $4in$ and $4out$ states is in a sense suppressed as a higher order process. (iii) Finally, quantum fluctuations result in a kinetic energy gain linear in transverse (‘quantum’) terms in the Hamiltonian for the monopoles, which is not present at this order in tetrahedra satisfying either $2in-2out$ or all-in or all-out correlations. This reduces the gap to single monopoles with respect to the gap to double monopoles (see also Ref. 11). The enhanced density of single monopoles at intermediate energies shows up in inelastic neutron scattering in quantum spin ice, which accounts for the rod-like motifs in Fig. 1.

In real compounds, inevitably, departures from ideal rods will be present, as a function of residual longer-range correlations. In particular, for long-range dipolar interactions, the size of which is appreciable especially for the large-spin canonical classical spin ices, pinch-point correlations persist¹³, albeit with an amplitude that vanishes with increasing temperature. The intermediate temperature range mentioned above will correspondingly exhibit some modulation along the rods, see e.g. Refs. 4 and 14.

Beyond this, in breathing pyrochlores, the exchange coupling can differ significantly between the two tetrahedral sublattices (J_1 and J_2)^{15–18}. Therefore, in a temperature regime where $J_1 \ll T \ll J_2$, the system is strongly correlated within tetrahedra in sublattice 2 and largely decoupled across tetrahedra in sublattice 1. There, we expect to observe well-formed rods (or the negative thereof) for ferromagnetic (antiferromagnetic) J_2 interactions.

In summary, we have accounted in a simple fashion for the appearance of rods in the neutron scattering data in a wide variety of settings in spin ice compounds and models. This includes the identification of a notable identity between the structure factor obtained at high temperature and the one from an uncorrelated sum over single tetrahedron lowest energy configurations.

In a broader context, it is natural to ask whether this also has implications for spins beyond the easy axis limit. Here, preliminary results indicate that this correspondence extends to a broader class of frustrated magnetic models. At the same time, the appearance of rods is not the only way for the pinch-points to disappear. In

frustrated continuous spin systems, it has recently been realised that another way of filling in the pinch-points leads to a different characteristic motif, namely that of half-moon pairs whose radii are energy-dependent^{19,20}.

Between them, these results not only provide signatures of the topological magnetism – and its disappearance – underpinning spin ice with its emergent gauge field, but they also establish such systems as enriching our collection of characteristic motifs – beyond Bragg peaks and broad paramagnetic features – in neutron scattering.

Acknowledgements. We are grateful to Akshat Pandey and Peter Holdsworth for useful discussions. This work was supported in part by EPSRC Grant No. EP/K028960/1 and EPSRC Grant No. EP/M007065/1 (CC) and by the Deutsche Forschungsgemeinschaft under grants SFB 1143 and EXC 2147 ct.qmat (RM).

Appendix A: Neutron Scattering details and single tetrahedron calculation

We consider unit-length spins pointing along their local $[111]$ easy axes, $\vec{S}_i = \sigma_i \hat{e}_i$, $\sigma_i = \pm 1$, where

$$\begin{aligned} \hat{e}_0 &= (1, 1, 1)/\sqrt{3} \\ \hat{e}_1 &= (-1, -1, 1)/\sqrt{3} \\ \hat{e}_2 &= (-1, 1, -1)/\sqrt{3} \\ \hat{e}_3 &= (1, -1, -1)/\sqrt{3}. \end{aligned} \quad (\text{A1})$$

The unpolarised neutron scattering cross section (up to the single ion form factor, which we ignore in this work) can be written as

$$\mathcal{F} = \sum_{\alpha, \beta = x, y, z} \left(\delta_{\alpha\beta} - \frac{k_\alpha k_\beta}{k^2} \right) \sum_{i, j} e^{i\vec{k} \cdot \vec{r}_{ij}} \langle S_i^\alpha S_j^\beta \rangle,$$

where $\vec{r}_{ij} = \vec{r}_j - \vec{r}_i$ and $k^2 = |\vec{k}|^2$. The $\vec{k} = 0$ point is ill-defined and should be disregarded. (As usual, if we were to consider polarised neutron scattering, the entirety of the signal would be in the spin-flip channel, whereas the non-spin-flip channel would give a featureless uniform background contribution.)

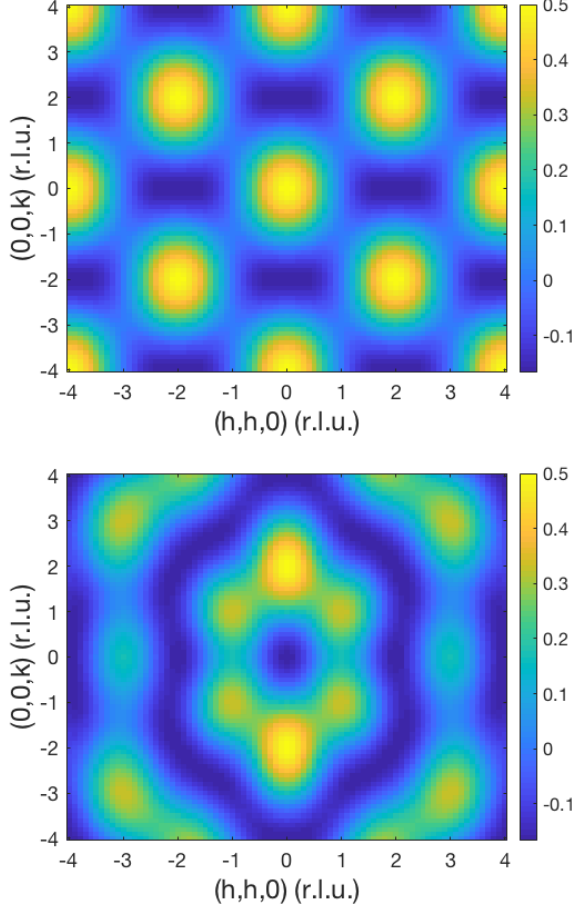


FIG. 3. Single tetrahedron calculation of the structure factor summed uniformly over all configurations but the all-in and all-out ones. Here we computed separately the two contributions to the neutron scattering transverse projector in Eq. (2), shown respectively in the top and bottom panel. The delta function contribution (top panel) corresponds to the conventional spin correlator, $\langle \vec{S}(\vec{q}) \cdot \vec{S}(-\vec{q}) \rangle$. Their sum gives the rods displayed in the right panel of the previous figure.

It is sometimes convenient to decompose \mathcal{F} into three contributions, a trivial one from $i = j$ (\mathcal{F}_0) and the two parts of the neutron scattering projector (\mathcal{F}_1 from $\delta_{\alpha\beta}$, and \mathcal{F}_2 from $-k_\alpha k_\beta / k^2$):

$$\mathcal{F}_0 = \sum_i \left[1 - \frac{(\hat{e}_i \cdot \vec{k})^2}{k^2} \right] = 2N_s/3 \quad (\text{A2})$$

$$\mathcal{F}_1 = -\frac{1}{3} \sum_{i \neq j} \cos(\vec{k} \cdot \vec{r}_{ij}) \langle \sigma_i \sigma_j \rangle \quad (\text{A3})$$

$$\mathcal{F}_2 = -\frac{1}{k^2} \sum_{i \neq j} (\hat{e}_i \cdot \vec{k})(\hat{e}_j \cdot \vec{k}) \cos(\vec{k} \cdot \vec{r}_{ij}) \langle \sigma_i \sigma_j \rangle, \quad (\text{A4})$$

where N_s is the total number of spins in the system.

The Fourier transforms are taken with respect to the

fcc lattice formed by one sublattice of tetrahedra. A conventional basis for this lattice can be written as $\vec{a}_1 = \ell(1, 0, 1)/2$, $\vec{a}_2 = \ell(1, 1, 0)/2$, and $\vec{a}_3 = \ell(0, 1, 1)/2$, where ℓ sets the unit length of the lattice (notice that, with this choice of normalisation, ℓ is the side of the cubic unit cell of the lattice). The reciprocal lattice basis vectors are $\vec{b}_1 = 2\pi(1, -1, 1)/\ell$, $\vec{b}_2 = 2\pi(1, 1, -1)/\ell$, and $\vec{b}_3 = 2\pi(-1, 1, 1)/\ell$. In real space, the nn distance on the pyrochlore lattice $r_{\text{nn}} = \ell/\sqrt{8}$ is customarily set to 1. However, in reciprocal space it is customary to work in so called reciprocal lattice units (r.l.u.), namely $\ell = 2\pi$, and we adopt this convention in the results presented in this work.

In a system of $L \times L \times L$ unit cells, the available points in the Brillouin Zone are spanned by $\vec{k} = m\vec{b}_1/L + n\vec{b}_2/L + p\vec{b}_3/L$, with $m, n, p = 0, \dots, L-1$. Namely,

$$\vec{k} = \frac{1}{L} (m + n - p, -m + n + p, m - n + p). \quad (\text{A5})$$

If we focus on the (h, h, k) plane, then $m = p$ and we are restricted to the points $\vec{k} = (n, n, 2m - n)/L$. It is then convenient to forego half of the points on the plane in exchange for a fully symmetric grid, and choose $n = 2i$ and $2m - n = 2j$, whereby $\vec{k} = 2(i, i, j)/L$. This is the choice adopted in all the Monte Carlo data presented in this work.

For a single tetrahedron, $N_s = 4$ and the $2^4 = 16$ configurations can be divided into three subsets: (i) 6 2in-2out states, where $\langle \sigma_i \sigma_j \rangle = -1/3$; (ii) 8 3in-1out or 3out-1in states, where $\langle \sigma_i \sigma_j \rangle = 0$; and (iii) 2 4in or 4out (aiao) states, where $\langle \sigma_i \sigma_j \rangle = 1$.

The separation vectors can be written as $\vec{r}_{ij} = \sqrt{3}\pi(\hat{e}_j - \hat{e}_i)/4$, in r.l.u. units where the pyrochlore lattice constant (i.e., the tetrahedron side) is $r_{\text{nn}} = 2\pi/\sqrt{8}$.

Given that $\mathcal{F} = 2N_s/3$ when summed trivially over all 16 configurations, and the same is true when projected onto the 3in-1out and 3out-1in configurations ($\langle \sigma_i \sigma_j \rangle = 0$), then we find the peculiar result that projecting onto the 2in-2out ice rule states gives an equal and opposite structure factor than projecting onto the aiao states. With a few lines of algebra, one obtains the explicit expressions

$$\mathcal{F}_1 = \frac{1}{6} [c_x c_y + c_y c_z + c_z c_x] \quad (\text{A6})$$

$$\mathcal{F}_2 = -\frac{1}{6} [c_x c_y + c_y c_z + c_z c_x] + \frac{1}{3k^2} [k_x^2 c_y c_z + k_z^2 c_x c_y + k_y^2 c_z c_x + k_x k_y s_x s_y + k_y k_z s_y s_z + k_z k_x s_z s_x], \quad (\text{A7})$$

where $c_\alpha = \cos(\pi k_\alpha/2)$ and $s_\alpha = \sin(\pi k_\alpha/2)$, for $\alpha = x, y, z$. Notice that, when the two contributions are summed together, \mathcal{F}_1 cancels exactly the first term in \mathcal{F}_2 and therefore, up to a trivial overall constant, the single tetrahedron neutron scattering structure factor is given by the last two lines in Eq. (A7) only.

-
- ¹ S. T. Bramwell and M. J. P. Gingras, *Science* **294**, 1495 (2001).
- ² C. Castelnovo, R. Moessner, and S. L. Sondhi, *Annu. Rev. Condens.Matter Phys.* **3**, 35 (2012).
- ³ S. V. Isakov, K. Gregor, R. Moessner, and S. L. Sondhi, *Phys. Rev. Lett.* **93**, 167204 (2004).
- ⁴ T. Fennell, P. P. Deen, A. R. Wildes, K. Schmalzl, D. Prabhakaran, A. T. Boothroyd, R. J. Aldus, D. F. McMorrow, and S. T. Bramwell, *Science* **326**, 415 (2009).
- ⁵ H. Kadowaki, N. Doi, Y. Aoki, Y. Tabata, T. J. Sato, J. W. Lynn, K. Matsuhira, and Z. Hiroi, *J. Phys. Soc. Japan* **78**, 103706 (2009).
- ⁶ C. Castelnovo, R. Moessner, and S. L. Sondhi, *Nature (London)* **451**, 42 (2008).
- ⁷ D. J. P. Morris, D. A. Tennant, S. A. Grigera, B. Klemke, C. Castelnovo, R. Moessner, C. Czternasty, M. Meissner, K. C. Rule, J.-U. Hoffmann, K. Kiefer, S. Gerischer, D. Slobinsky, R. S. Perry, *Science* **326**, 411 (2009).
- ⁸ K. Kimura, S. Nakatsuji, J.-J. Wen, C. Broholm, M.B. Stone, E. Nishibori and H. Sawa, *Nature Communications* **4**, 1934 (2013).
- ⁹ S. Petit, E. Lhotel, B. Canals, M. Ciomaga Hatnean, J. Ollivier, H. Mutka, E. Ressouche, A. R. Wildes, M. R. Lees and G. Balakrishnan, *Nature Physics* **12**, 746 (2016).
- ¹⁰ S. Petit, E. Lhotel, S. Guitteny, O. Florea, J. Robert, P. Bonville, I. Mirebeau, J. Ollivier, H. Mutka, E. Ressouche, C. Decorse, M. Ciomaga Hatnean, and G. Balakrishnan, *Phys. Rev. B* **94**, 165153 (2016).
- ¹¹ Y. Kato and S. Onoda, *Phys. Rev. Lett.* **115**, 077202 (2015).
- ¹² N. P. Raju, M. Dion, M. J. P. Gingras, T. E. Mason, and J. E. Greedan, *Phys. Rev. B* **59**, 14489 (1999).
- ¹³ A. Sen, R. Moessner, S. L. Sondhi, *Phys. Rev. Lett.* **110**, 107202 (2013).
- ¹⁴ L. J. Chang, Y. Su, Y.-J. Kao, Y. Z. Chou, R. Mittal, H. Schneider, Th. Brückel, G. Balakrishnan and M. R. Lees, *Phys. Rev. B* **82**, 172403 (2010).
- ¹⁵ Y. Okamoto, G. J. Nilsen, J. P. Attfield, and Z. Hiroi, *Phys. Rev. Lett.* **110**, 097203 (2013).
- ¹⁶ Y. Tanaka, M. Yoshida, M. Takigawa, Y. Okamoto, and Z. Hiroi, *Phys. Rev. Lett.* **113**, 227204 (2014).
- ¹⁷ R. Saha, F. Fauth, M. Avdeev, P. Kayser, B. J. Kennedy, and A. Sundaresan, *Phys. Rev. B* **94**, 064420 (2016).
- ¹⁸ S. Lee, S.-H. Do, W.-J. Lee, Y. S. Choi, M. Lee, E. S. Choi, A. P. Reyes, P. L. Kuhns, A. Ozarowski, and K.-Y. Choi, *Phys. Rev. B* **93**, 174402 (2016).
- ¹⁹ H. Yan, R. Pohle, and N. Shannon, *Phys. Rev. B* **98**, 140402(R) (2018).
- ²⁰ T. Mizoguchi, L. D. C. Jaubert, R. Moessner, and M. Udagawa, *Phys. Rev. B* **98**, 144446 (2018).